# Flame Edge Dynamics and Interaction in a Multinozzle Can Combustor With Fuel Staging

**Daniel Doleiden**
Department of Mechanical Engineering,
Pennsylvania State University,
University Park, PA 16802

**Wyatt Culler**[1]
Department of Mechanical Engineering,
Pennsylvania State University,
University Park, PA 16802

**Ankit Tyagi**
Department of Mechanical Engineering,
Pennsylvania State University,
University Park, PA 16802

**Stephen Peluso**
Department of Mechanical Engineering,
Pennsylvania State University,
University Park, PA 16802

**Jacqueline O'Connor**
Department of Mechanical Engineering,
Pennsylvania State University,
University Park, PA 16802

*The characterization and mitigation of thermoacoustic combustion instabilities in gas turbine engines are necessary to reduce pollutant emissions, premature wear, and component failure associated with unstable flames. Fuel staging, a technique in which the fuel flow to a multinozzle combustor is unevenly distributed between the nozzles, has been shown to mitigate the intensity of self-excited combustion instabilities in multiple nozzle combustors. In our previous work, we hypothesized that staging suppresses instability through a phase-cancelation effect in which the heat release rate from the staged nozzle oscillates out of phase with that of the other nozzles, leading to destructive interference that suppresses the instability. This previous theory, however, was based on chemiluminescence imaging, which is a line-of-sight integrated technique. In this work, we use high-speed laser-induced fluorescence to further investigate instability suppression in two staging configurations: center-nozzle and outer-nozzle staging. An edge-tracking algorithm is used to compute local flame edge displacement as a function of time, allowing instability-driven edge oscillation phase coherence and other instantaneous flame dynamics to be spectrally and spatially resolved. Analysis of flame edge oscillations shows the presence of convecting coherent fluctuations of the flame edge caused by periodic vortex shedding. When the system is unstable, these two flame edges oscillate together as a result of high-intensity longitudinal-mode acoustic oscillations in the combustor that drive periodic vortex shedding at each of the nozzle exits. In the stable cases, however, the phase between the oscillations of the center and outer flame edges is greater than 90 deg (~114 deg), suggesting that the phase-cancelation hypothesis may be valid. This analysis allows a better understanding of the instantaneous flame dynamics behind flame edge oscillation phase offset and fuel staging-based instability suppression.*
[DOI: 10.1115/1.4044230]

## Introduction

Lean premixed combustors facilitate efficient combustion of natural gas with lower $NO_x$ emission levels [1]. However, such combustors are susceptible to combustion instability, a thermoacoustic feedback process [2]. This feedback loop manifests when acoustic oscillations drive heat release rate oscillations, a result of local equivalence ratio and convective velocity fluctuations driven by the acoustics. Thus, when an in-phase relationship between local heat release rate oscillations and the natural acoustic mode of a combustor is obtained, the thermoacoustic feedback loop is strengthened and appreciable energy is transferred to the acoustic field [3].

From an operability standpoint, mitigation of combustion instability is necessary to reduce convective heat transfer to internal components, the potential for flashback and blow-off, and acoustic vibratory loads. Various control methods have been proposed and implemented industrially [4,5]. In almost all operational gas turbines, passive methods of control are used, as these methods may be implemented during the design phase to tailor the combustor's acoustic response or added after to mitigate unforeseen issues.

A commonly used passive strategy called fuel staging involves redistribution of fuel flow to different nozzles within a multinozzle combustor as a means of interrupting the instability feedback cycle. Fuel staging has been shown to be effective in industrial gas turbines, including the Siemens SGT-200 industrial gas turbine [6,7] and in the GE DLN-2.6 combustion system [8]. Studies of fuel staging have shown that the primary effect of fuel staging is to redistribute the heat release inside the combustor, which can have a number of effects on the instability. Work by Li et al. [9] showed, through a numerical simulation of a Rijke tube combustor, that nonuniformity of the heat release could drive vortical waves in the combustor that decreased the amplitude of the instability growth rate.

A larger literature on nonuniform heat release rate effects exists for annular combustor systems, where transverse modes are more common than in can combustor systems. A symmetry-breaking argument was made by Cohen et al. [10] in an annular combustor, where they showed that the driving of the transverse mode was inherently linked to the symmetry of the heat release rate around the annulus. Numerous theoretical investigations have shown the effect of nonuniform heat release rate in annular combustors, including work by Noiray et al. [11,12], Ghirardo and Juniper [13], Acharya et al. [14], and Li et al. [15], but these studies typically do not model detailed flame dynamics and so the flame mechanisms by which instability is suppressed with nonuniform heat release rate distributions is still unclear. Additionally, the mechanism for suppression of a transverse mode is likely different than that of a longitudinal mode, particularly when comparing an annular and a can combustor where the cut-on frequencies for the transverse and longitudinal modes are very similar in annular systems but can be an order of magnitude different in can systems.

Literature detailing the mechanism by which fuel staging stabilizes the combustor is sparse, despite the growing literature on multinozzle combustor systems [16–20]. We have previously shown that the in-phase oscillation of adjacent flames in the unstable regime suggests the presence of large-scale, coherent vortical structures that convect downstream from the combustor dump plane [21]. Examination of local instantaneous heat release rate phase via chemiluminescence imaging showed these oscillations to occur in-phase with dynamic pressure sampled at the dump plate [22], illustrating two components of the instability feedback loop. In the stable regime, the staged flame seemed to oscillate out of phase with the other flames, as evidenced by a shift in the local

[1]Present address: Honeywell Thermal Solutions, Muncie, IN 47307.

Manuscript received June 27, 2019; final manuscript received July 11, 2019; published online August 2, 2019. Editor: Jerzy T. Sawicki.

phase oscillations of adjacent flames and a significant reduction in the pressure fluctuation amplitude. Thus, we proposed that fuel staging breaks the instability feedback loop by de-phasing the oscillations of the staged flame relative to the other flames, reducing the global heat release rate oscillations and suppressing energy input to the acoustic field.

Recently, we showed that axisymmetric fuel staging can provide similar levels of instability suppression as nonaxisymmetric fuel staging [23]. In this experiment, we varied the fuel staging to all five nozzles separately and compared the pressure root-mean-square (RMS), chemiluminescence RMS, and instantaneous phase between the chemiluminescence oscillations and the pressure oscillations (via a Hilbert transform) to understand the differences in staging with different nozzles. Additionally, we identified the "bifurcation equivalence ratio," or the staging equivalence ratio required in each nozzle to suppress the instability; it varied between the center nozzles and three of the four outer nozzles. An apparent difference in effectiveness between the center nozzle and one of the outer nozzles was attributed to minor nozzle hardware variations.

The chemiluminescence imaging technique used in these two previous studies is limited in that it is a line-of-sight integrated technique, which does not provide spatial resolution of flame edge structure or localized phenomena [24]. Another imaging-based diagnostic technique, OH-radical planar laser-induced fluorescence (OH-PLIF), excites OH radicals within a thin laser sheet. The excited OH radicals then fluoresce at a known wavelength. In conjunction with a high-speed camera, this method produces images with high spatial and temporal fidelity. Here, OH-PLIF images taken across the centerline of adjacent flames were used to understand local flame interaction dynamics.

In this work, we utilize OH-PLIF and an edge tracking algorithm to investigate the previously proposed hypothesis that fuel staging suppresses instability via flame oscillation phase cancelation. We consider two cases—center-nozzle staging, which has been shown to repeated suppress instability, and right-nozzle staging, which is our experiment did not suppress the instability as the other nozzles [23]. In particular, the right nozzle had a higher bifurcation equivalence ratio than the center nozzle, which means that it required more fuel staging than the other four nozzles to adequately suppress instability. This difference in staging efficacy between nozzles is apparent in both the pressure fluctuation amplitude as well as the dynamics of the flame in the OH-PLIF imaging.

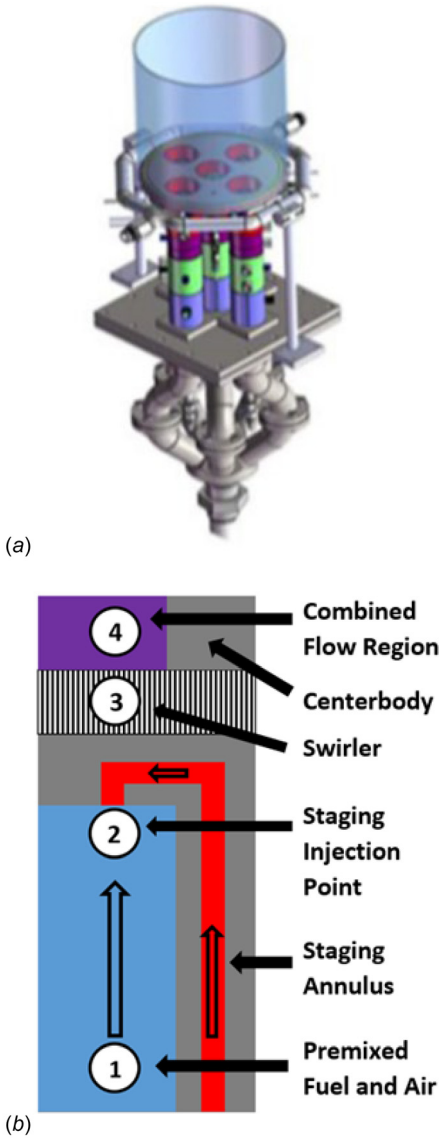


**Fig. 1 (*a*) The multinozzle combustor and (*b*) a cross section of the staged nozzle showing (1) flow of premixed fuel and air, (2) injection of staging fuel, (3) swirler, and (4) the combined flow region**

## Experimental Setup and Methods

**Experimental Configuration.** Experiments are conducted in a laboratory-scale four-around-one multinozzle can combustor, shown in Fig. 1(*a*), which has been previously described in Refs. [21] and [22]. This combustor confines atmospheric pressure premixed natural gas–air flames anchored to annular swirler nozzles within an optically accessible 25.4 cm diameter cylindrical quartz chamber with an open, pressure-release boundary condition at the exit. A representative nozzle cross section is provided in Fig. 1(*b*); actual nozzle geometry is proprietary, but this sketch shows the key flow passages within the nozzle and how the fuel and air are mixed in the swirler vanes.

Compressed air is preheated to 200 °C via a 50 kW process heater (Tempco) and mixed with natural gas to form a 200 psi premixed bulk mixture, which is supplied to each nozzle at equal flowrates via a manifold. A nominal thermal output of approximately 220 kW is produced by fuel and air flowrates of 452 SLM and 7162 SLM, respectively. These flow rates result in a nozzle bulk velocity of 26 m/s.

Modification of the equivalence ratio of the fuel/air mixture produces self-excited instability; the first quarter-wave longitudinal mode is unstable at approximately 530 Hz and no other modes are present at the conditions in this study. The combustor is thermoacoustically unstable when all nozzles are fueled at an equivalence ratio of 0.7 and above. A more detailed discussion of the stability map of this experiment is in Samarasinghe et al. [21], but only variations around the stability bifurcation point at an equivalence ratio of 0.7 were considered here. The unstable condition of the combustor is defined by a dump plane pressure variation RMS ($P'_{\mathrm{RMS}}$) of greater than 0.5 kPa (0.05% of the mean combustor pressure). Additionally, instability tonality is ensured by requiring a 12 Hz bin centered about the instability frequency to have an amplitude greater than 30 times that of the noise floor. The dump plane pressure signal frequency resolution for all experiments is 0.0625 Hz.

An analog solenoid valve (Humphrey ProControl PC3) actuates an auxiliary fuel delivery system that permits fuel staging by injection of natural gas in the fuel circuit of each nozzle. This staging flow represents approximately 5% of the total fuel flow rate. As shown in Fig. 1(*b*), the bulk mixture flows through the annulus of each nozzle, with staging fuel injected upstream of the swirler of the selected nozzle. Previous measurements [25] demonstrated that the bulk and staging flows are thoroughly mixed ahead of the nozzle orifice.

When fuel staging is applied, the equivalence ratio of the staging nozzle increases, while the equivalence ratio of the other four nozzles decreases since all fuel circuits are connected to a common source; as such, fuel staging is largely a redistribution of the fuel rather than a significant change in the global equivalence ratio. However, staging does increase global equivalence ratio slightly, resulting in global equivalence ratios in the range between 0.71 and 0.72, depending on staging level. Self-excited instability is present at these global equivalence ratios without staging. Instability suppression is achieved when the global equivalence ratio is held constant and staged nozzle equivalence ratio is increased to 0.80 (in the center nozzle) or 0.85 (in the right nozzle); these differences in the staging efficacy were detailed in Culler et al. [23]. The fuel staging system enables the equivalence ratio of a selected nozzle to be modified in increments of approximately 0.01. A National Instruments data acquisition system is used for staging solenoid control and thermal and pressure data acquisition.

Air flowrate control is provided by a manual needle valve and a Sierra Instruments 760S flowmeter. Bulk fuel flowrate is controlled with a manual needle flowrate and a Teledyne-Hastings HFM-301 flowmeter. Staging flowrate is measured by a Teledyne-Hastings HFM-201 flowmeter and is solenoid controlled.

**Diagnostics.** Type K thermocouples sense dump plane and nozzle center body temperatures throughout each experiment. The temperature at these locations is registered at the beginning and ending of each run to ensure consistent thermal conditions between tests. A water-cooled dynamic pressure transducer mounted in a recess on the dump plane samples dynamic pressure. Pressure and thermal data are collected at 16,384 Hz; a 10 Hz high-pass filter is applied to eliminate low frequency noise induced by vibration of the pressure transducer.

OH planar laser-induced fluorescence is used to visualize ground-state hydroxyl radicals within a laser sheet, allowing flame edges to be defined with high spatial and temporal fidelity. A pump laser (Edgewave Innoslab IS200-2 L Nd:YAG diode laser) is used with a rhodamine chloride dye laser (Sirah Credo high-speed dye laser) to produce an approximately 2.0 W beam. The beam is pulsed at 10 kHz with a pulse energy of approximately 0.2 mJ/pulse at 282 nm. Images are taken at 10 kHz via high-speed camera (Photron SA 1.1) equipped with an intensified relay optic (LaVision HS-IRO) and a UV lens (Cerco 100 mm f/2.8). A 320 nm filter (LaVision 1108760 VZ-Image) isolates OH fluorescence emissions.

An optical chain consisting of UV mirrors, positive and negative cylindrical lenses, and a periscope is used to steer and collimate the laser beam into a vertical sheet approximately 40 mm high. In this paper, we discuss results measured in a 20 mm sheet located near the dump plane to capture the dynamics of the flame near its attachment point; two other fields of view were measured downstream, but the results are not presented here due to lower signal quality. The field of view analyzed in this study is in Fig. 2, which shows a time-averaged chemiluminescence image of the flames with the sheet location and field of view overlaid on top.

A National Instruments LABVIEW interface facilitates the data collection process by providing data acquisition system communication, staging solenoid control, and high-speed camera triggering in tandem with DAVIS control software (V 8.3.1) and LaVision high speed and IRO controllers. Before each experiment, the laser system is brought to full power and the desired fuel and air flow rates are set. The LABVIEW interface then initiates the experiment, sampling thermal and pressure data, opening or closing the staging solenoid, and triggering high-speed camera recording.

**Data Analysis.** A MATLAB-based edge tracking algorithm is used to locate flame edges on a per-frame basis. A modified version of Otsu's method [26] is used to binarize the images with adjustable high and low saturation thresholds. Bicubic noise reduction and laser sheet profile corrections are used to improve image quality. Flames are detected and registered as objects within each successive binarized frame and the right edge of the center flame and the left edge of the right flame are identified.

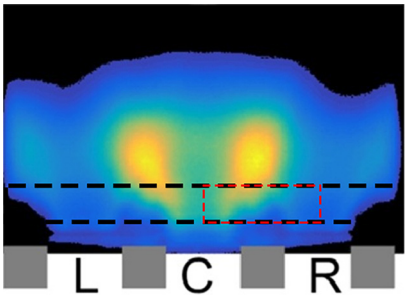


**Fig. 2 Time-averaged chemiluminescence image of the combustor. Black dashed lines denote laser sheet bounds. Red dashed lines denote LIF image field of view. Gray blocks indicate nozzle boundaries. Left (L), center (C), and right (R) flame locations marked (See color figure online).**

We quantify the oscillations in the flame surface area, which drive the instability feedback loop during velocity-coupled instability [27], by measuring the lateral displacement of the flame edge. This technique is similar to analysis by Shanbhogue et al. [28], who analyzed the dynamics of bluff-body stabilized flames under acoustic forcing, enabling them to determine the factors contributing to coherent flame response. In lieu of a direct local heat release rate measurement technique, we study local flame edge displacement and wrinkling, which is a good indicator of heat release rate fluctuations during longitudinal instability. In previous work [29], heat release rate oscillations were quantified through chemiluminescence imaging, which is a line-of-sight integrated technique. Although it provided some insight into the mechanism by which fuel staging suppresses instability, it cannot provide information about local or instantaneous flame dynamics, which the LIF technique can. As the flame oscillates laterally, a result of vortex rollup in the shear layers excited by the longitudinal acoustic mode, the flame sheet area oscillates as well; comparisons between this technique and flame area tracking using level-set methods [28,30] even at high turbulence intensities [31,32], have shown good agreement between flame displacement and flame area metrics. The edge displacement time series ($L'$) is constructed by tracking the lateral displacement of the flame edges as a function of downstream distance and time. A fast Fourier transform is performed on $L'$ enabling the calculation of flame edge oscillation phase and flame edge oscillation RMS at the instability frequency at each location downstream.

The accuracy of the edge tracking algorithm has been verified by overlaying the identified edges on raw LIF images. This algorithm only accounts for lateral oscillations in the flame and does not consider the multivalued nature of the flame edge, which can occur during high-amplitude flame wrinkling due to vortex rollup. When the flame is multivalued at a certain downstream location, the flame edge farthest from the centerline is chosen.

## Results

**Time-Averaged Flame Structure.** A total of three operating conditions were considered in this study: unstaged unstable, center-nozzle-staged stable, and right-nozzle-staged stable; there are two repeats of each case. For all cases, a baseline equivalence ratio of 0.70 was set for all unstaged nozzles, with staged nozzles operated at a richer equivalence ratio of 0.85. A test matrix is provided in Table 1.

The time-averaged flame shape at each condition is visualized using the flame surface density (FSD), which is obtained by calculating the mean of instantaneous flame edge location across all

**Table 1 Test matrix**

| Mode | Staged nozzle equivalence ratio | Unstaged nozzles equivalence ratio | Instability amplitude (psi) |
|---|---|---|---|
| Unstaged unstable | 0.70 | 0.70 | 0.25 |
| Center-nozzle staged stable | 0.85 | 0.69 | 0.01 |
| Right-nozzle staged stable | 0.85 | 0.69 | 0.05 |

LIF image frames within a given time period. Flame surface density plots provided in Fig. 3 show both the anchoring of the flame and some indications of the dynamics. Above each nozzle, a total of four separate branches are visible. The inner branches correspond to the V-shaped anchored flame, and the outer branches correspond to the recirculation zones, which are situated between adjacent flames and between flames and the combustor liner. The FSDs also show that both center- and right-nozzle staging reduce the severity of flame branch oscillation associated with instability. This observation is demonstrated by comparing the width of the flame brush in each of these cases; the flame brush is markedly thinner in the center-staging and right-staging cases as compared to the unstable case.

**Time-Varying Flame Dynamics.** A series of instantaneous LIF images depicting the left branch of the right-nozzle flame (RL branch) and the right branch of the center-nozzle flame (CR branch) are provided in Fig. 4. The flames are attached to recessed center bodies, shown by the cross-hatched regions on the far left and far right sides of the bottom image, and a small recirculation zone forms behind the dump plane between the flames. Large-scale flame wrinkling, a result of vortex formation, roll-up, and convection, is observed on both flame branches during instability, resulting in enhancement of flame surface area. Though the OH-PLIF image cannot provide direct evidence of the vortex, the large-scale wrinkling has been shown to be a result of this velocity-coupling mechanism in previous studies [9]. Specifically, simultaneous oscillation of the instantaneous flame edge location indicates vortex formation and shedding occurs coherently between the RL and CR branch. Arrows in the second column of images in Fig. 4 mark the formation and shedding cycle of vortical structures across a 0.5 ms timespan. During vortex formation and roll-up, large magnitude oscillations occur in $L'$ for both the RL and CR flame branches. As a vortex forms and convects past the lower boundary of the laser sheet and into view, the location of both flame edges is shifted away from the recirculation region situated between the flames. As the vortex convects further downstream, the flame edges oscillate outward. Approximately two cycles of vortex shedding are shown in the images in Fig. 4, which should be read top to bottom, left to right. The flame branches oscillate in and out together as a result of the longitudinal instability, which creates simultaneous vortex shedding in both nozzles.

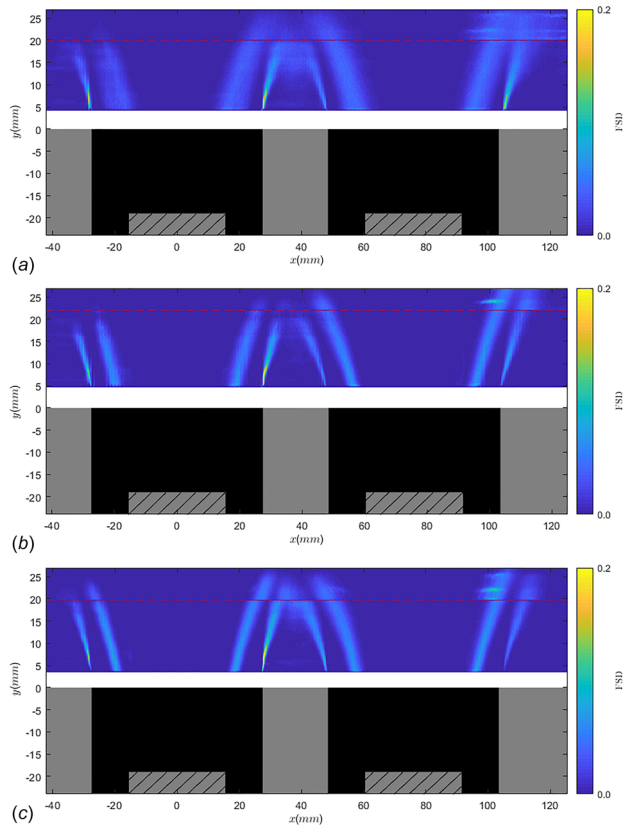


**Fig. 3 FSD plots for (*a*) unstaged unstable, (*b*) right-nozzle staged, and (*c*) center-nozzle staged operating modes**

Fuel staging changes the instantaneous vortex dynamics and flame branch oscillations; instantaneous LIF image time series presented in Fig. 5 show both the right-nozzle and center-nozzle staged cases. As indicated by arrows, the right-nozzle staged time series shows the continued presence of coherent flame edge oscillations with right-nozzle staging, albeit with appreciably subdued magnitude compared to the unstaged operating mode. The center-nozzle staged time series shows that coherent flame edge oscillation is almost eliminated with center-nozzle staging.

Fuel staging is expected to have several different effects on the flames and their behavior due to the changing equivalence ratio of each flame; the equivalence ratio of the staged flame increases and that of the other flames decreases. First, the shape of the flames changes, as can be seen in the flame surface density plots in Fig. 3. In particular, we expect that the center of heat release for the staged flame moves upstream (due to the increase in flame speed) and that of the other flames moves downstream (due to the decrease in flame speed). We show next that this change in flame structure results in phase differences between the heat release rate oscillations of adjacent flames.

Additionally, the overall heat release rate from each flame changes accordingly with the equivalence ratio. This means that heat release rate oscillations from each flame, normalized by the time-averaged heat release rate, will differ in each flame given the same input. This change in the equivalence ratio will change the amplitude of driving each flame can add to the thermoacoustic feedback cycle. The details of these changes are quantified in the next section by analyzing the changes to the flame oscillation amplitude and phase for adjacent flames.

**Quantification of Flame Dynamics.** The local flame dynamics are quantified using the flame edge oscillation amplitude ($L'$) and phase ($\varphi$) along the CR branch and the RL branch for all modes, shown in Fig. 6. Here, Fig. 6(*a*) shows $L'_{\mathrm{RMS}}$ as a function of downstream distance for both flame branches, and Fig. 6(*b*) shows the phase of the flame edge oscillations. The spectral densities of the $L'$ oscillation at approximately 10 mm downstream of the nozzle and those of the combustor pressure oscillation are in Fig. 7. These spectra provide some idea of the coherence of the oscillations relative to the background noise. To interpret the phase, it should be noted that if the flames are oscillating together (as a result of simultaneous vortex shedding), the phase between the edges will be $\pi$ radians, as the vortices push the center flame to the right and the right flame to the left. As such, oscillations of the flame edges out of phase to create cancelation are represented by a relative phase of 0 rad. The slope of the phase is indicative of the wrinkle convection speed along the flame edge, which should be similar to the bulk flow velocity, but not necessarily equal to it [33]. The wrinkle convection speed is 22.3 m/s for the CR branch and 23.9 m/s for the RL branch, whereas the bulk velocity is 26 m/s.

As shown in Fig. 6, both the RL and CR flame branches of the unstable flames exhibit relatively large $L'_{\mathrm{RMS}}$ values, varying

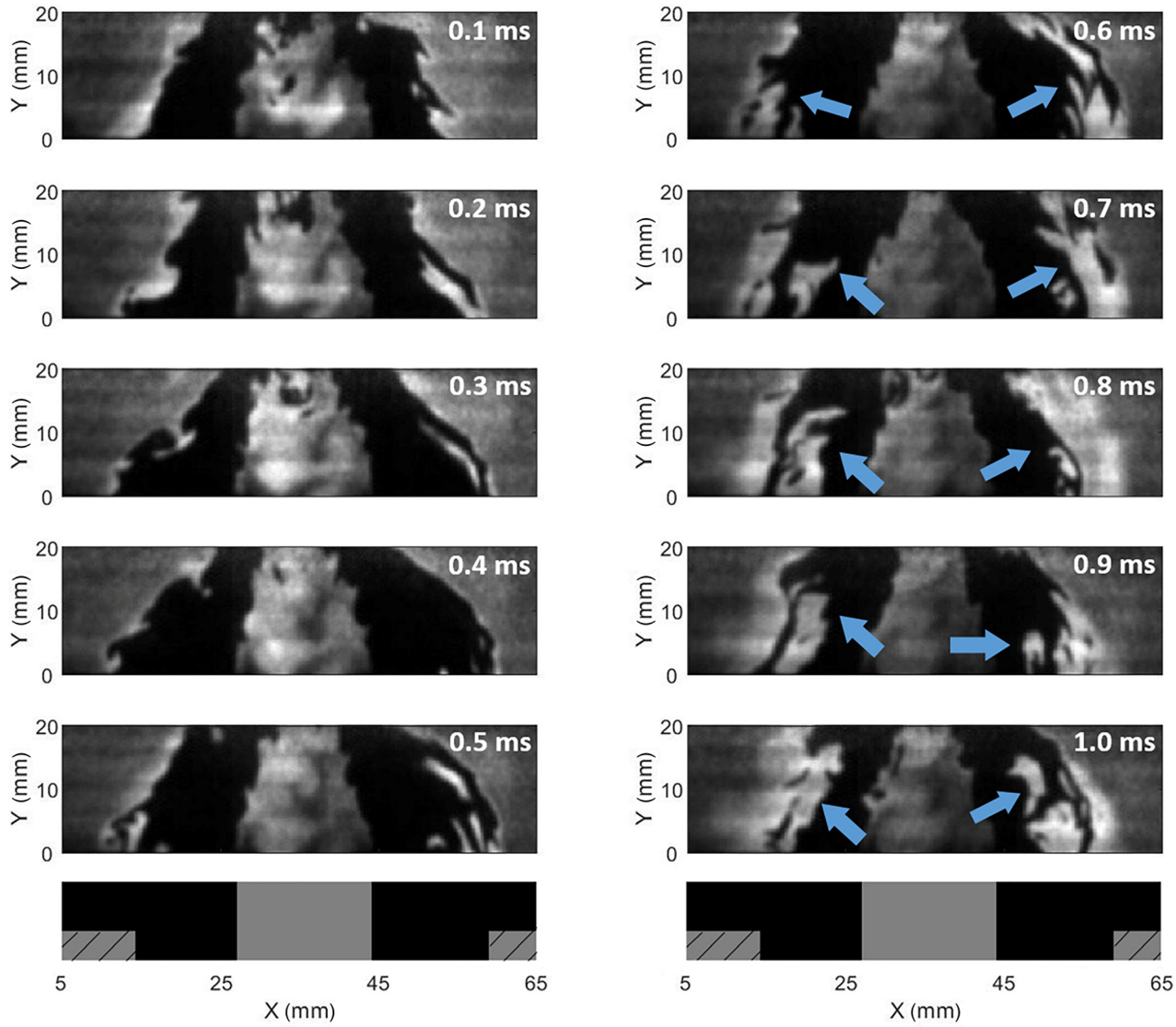


**Fig. 4 Instantaneous LIF image time series of unstable operating mode. Left to right: center flame, recirculation zone, right flame. Timestep = 0.1 ms ordered vertically.**

between approximately 1.5 and 2.5 mm as a function of downstream distance. These oscillations occur with a mean phase offset of approximately $1.3\pi$ rad, indicating that simultaneous vortex shedding is present in the two flames. Single-sided power spectral densities in Fig. 7(*a*) show that $L'$ and $P'$ peak at identical frequencies, indicating coupling between vortex shedding and pressure fluctuation. Also, the signal-to-noise ratio in both spectra is very high, indicating high coherence of the oscillations.

A similar analysis is presented for the right-nozzle staged case and the center-nozzle staged case. In Fig. 6, the $L'_{\mathrm{RMS}}$ values of the right-nozzle staged case are markedly lower than those of the unstable case and they have a phase offset of approximately $0.75\pi$ radians, indicating the presence of lower amplitude flame wrinkling as compared to the unstable case. Single-sided power spectral densities (Fig. 7(*b*)) have an identical frequency peak to the unstable case, although the amplitude is lower as a result of the partially suppressed instability.

In the center-nozzle staged case, $L'_{\mathrm{RMS}}$ values are notably lower than those of both the right-nozzle staged case and unstaged case. The phase offset is close to zero, indicating that flame edge oscillations are out of phase, resulting in possible phase cancelation. Single-sided power spectral densities (Fig. 7(*c*)) show that $L'$ and $P'$ no longer exhibit high-amplitude frequency peaks, indicating that the feedback cycle between flame edge fluctuation and pressure fluctuation weakens with center nozzle staging. In this case, the phase offset should be interpreted with care. As the amplitude of the signal approaches zero, the phase is not a meaningful quantity. If this limit had been reached, we would expect the phase to be a random quantity; however, the phase at subsequent downstream distances displays continuity, suggesting that there is some coherence remaining and that we can tentatively extract conclusions from the phase relationship between the left and right branches, even at this low oscillation amplitude. At the higher $L'_{\mathrm{RMS}}$ values, more in-phase oscillation of $L'$ and increased $L'$–$P'$ coherence of the right-nozzle staged case compared to the center-nozzle staged case captures the reduced "efficacy" and presence of damped coherent oscillations associated with right-nozzle staging at the prescribed equivalence ratios.

Box plots of the phase offset ($\Delta\varphi$) between the CR and RL flame branches for two examples of each operating mode are provided in Fig. 8. These plots denote the median of each data set with a horizontal line; the inner quartile range, limited by the 25th and 75th percentiles, is represented by a box enclosing the median. Vertical dashed whiskers extending from the boxes denote the lowest and highest values of points not considered outliers, and outliers are represented by plus signs above and below the whiskers. Outliers are identified as points that lie outside 1.5 times the inner quartile range [34]. Ninety-one points along the

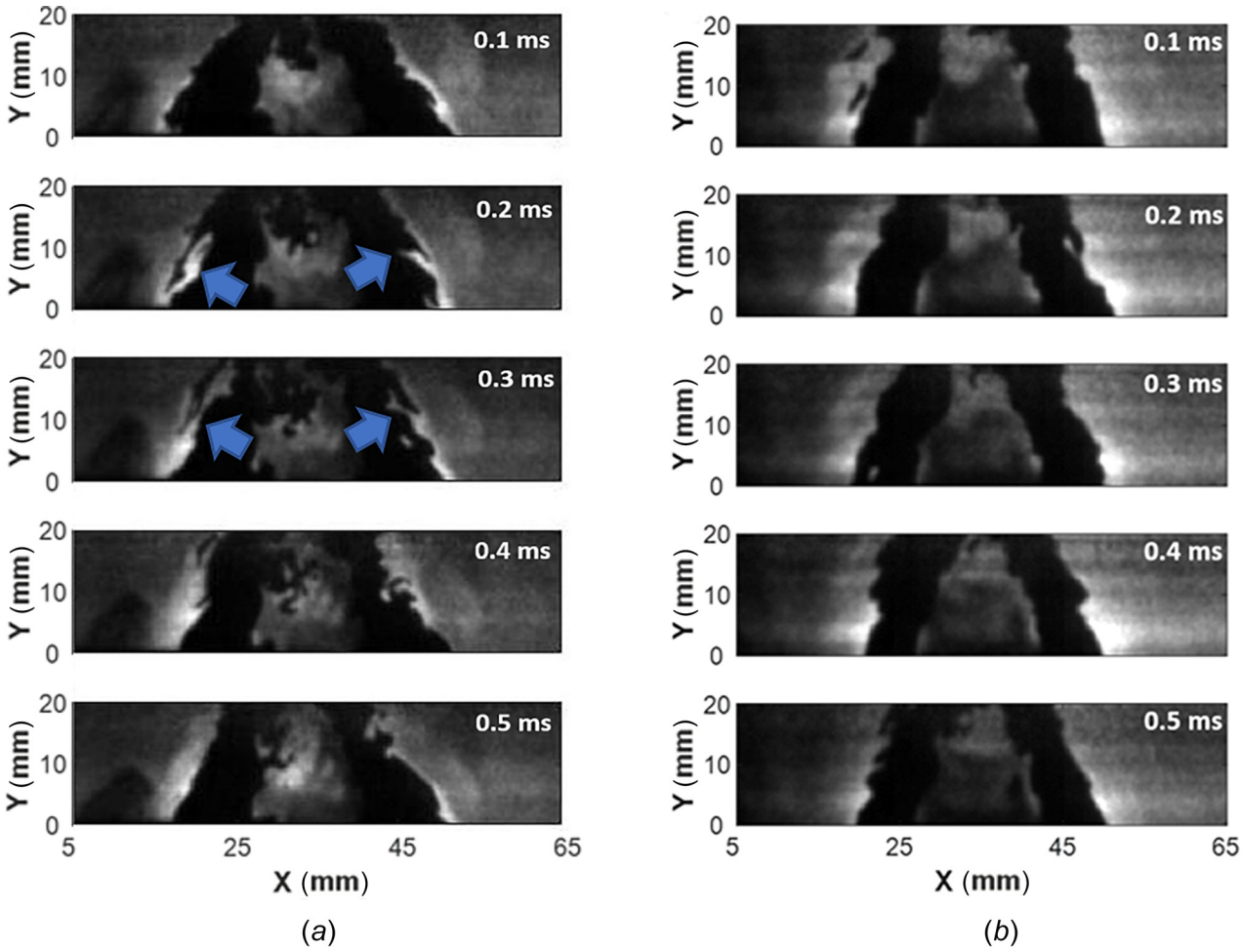


**Fig. 5 Instantaneous LIF image comparison of (*a*) right- and (*b*) center-nozzle staging. Timestep = 0.1 ms ordered vertically.**

flame are used for the unstable cases, while the right-nozzle staged and center-nozzle staged cases have 86 and 79 points along the flame, respectively. The boxplots show the variation in local phase oscillations between branches as a function of downstream distance.

As previously mentioned, local $L'$ oscillations are considered out-of-phase when $\varphi$ is between 0 and $0.5\pi$ radians, and in-phase when $\varphi$ is between $0.5\pi$ and $1.5\pi$ radians. The medians in Fig. 8 show that the unstaged unstable and right-nozzle staged cases exhibit constructive edge oscillation interference, while the center-staged cases effectively neutralize this coherence. The relatively low spread of the boxes in Fig. 8 corresponding to the unstaged and right-nozzle staged cases demonstrates the higher degree of coherence observed in these operating modes; a markedly higher spread (and thus lower degree of coherence) is present in the center-nozzle staged cases. The intermittent formation of small-scale vortices, such as those shown on the RL branch during right-nozzle staging in Fig. 5, contributes to the presence of outliers in Fig. 8. The presence of strong edge oscillation coherence and persistent pressure intermittency in the right-nozzle staged operating mode is further evidence that the aforementioned damped coherent oscillation state [22] has been reproduced.

The intermittency in the combustor pressure and flame edge oscillation level, resulting in the spread in the data for the right-staged and center-staged cases, is driven by intermittency in the phase of oscillation between the center and right flames. Figure 9 shows time-series data of the dump plane pressure for the unstable (Fig. 9(*a*)), right-staged (Fig. 9(*b*)), and center-staged (Fig. 9(*c*)) cases. In the unstable case, the RMS amplitude of the instability is relatively stationary for long time durations (as compared to the instability frequency). However, there is higher levels of intermittency in the pressure fluctuation amplitudes for the staged cases. In particular, the right-nozzle staging case has an intermittent pressure amplitude, a result of the less effective staging by that nozzle. In this time signal, intermittent bursts of higher oscillation amplitude are seen, some of which last for almost a second (7–7.8 s). This level of intermittency in the instability amplitude is common for unstable systems near their bifurcation point. Smaller bursts of higher-amplitude oscillations can be seen in the center-staged case, but overall the instability amplitude is both lower and more stable.

Figure 10 provides $L'$ time series of both the right branch of the center flame and the left branch of the right flame for each operating mode filtered in a 25 Hz band around the instability frequency. Observing the data in this way helps to better visualize the relative phase between oscillations on each flame branch. In the time series of the unstable case (Fig. 10(*a*)), the edges are continuously oscillating out of phase, which is indicative of the two flames undergoing simultaneous flame wrinkling due to large-scale vortex shedding at the instability frequency. In the two staging cases, however, the phase between the two signals drifts between in-phase and out-of-phase oscillations, with more switching in the right-staged case (Fig. 10(*b*)) than in the center-staged case (Fig. 10(*c*)). The in-phase oscillations are evidence of the phase-cancelation hypothesis that was proposed to explain the mechanism by which fuel staging suppresses instability in the multinozzle combustor. However, the instantaneous phase between the two flame edges drifts with time, which results in some ambiguity in the overall phase shown in Fig. 6.

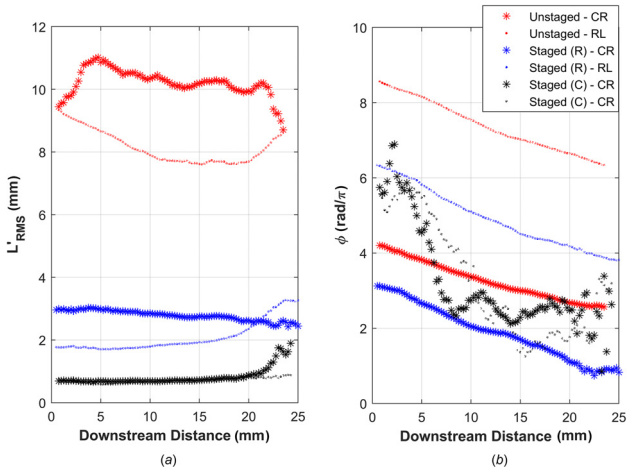


**Fig. 6 (*a*) $L'_{RMS}$ and (*b*) $\phi$ for all operating modes**

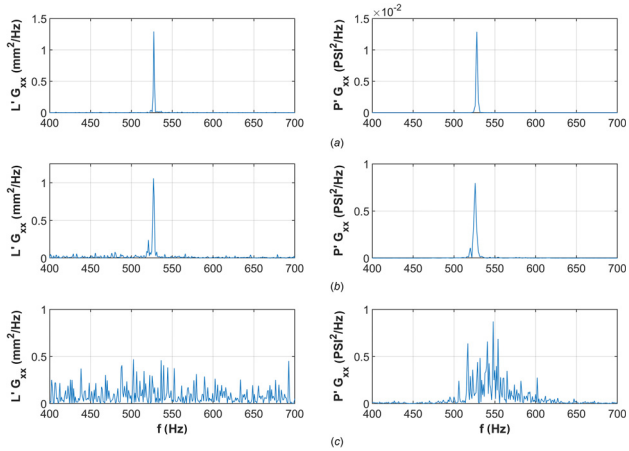


**Fig. 7 Single-sided power spectral density of $L'$ and $P'$ for (*a*) unstaged unstable, (*b*) right-nozzle staged stable, and (*c*) center-nozzle staged stable operating modes**

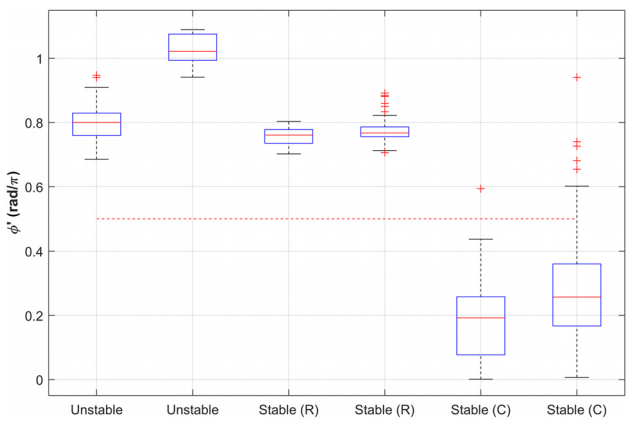


**Fig. 8 Box plots of $\phi$ for unstable unstaged, stable right-staged (R), and stable center-staged (C) operating modes. Dashed lines demarcates the in-phase and out-of-phase regions.**

## Conclusions

This study examined vortex formation and roll-up, edge oscillation, and interflame edge relations in a multinozzle can combustor under unstable, stable axisymmetric (center nozzle) staged, and marginally stable nonaxisymmetric (right nozzle) staged operating modes via edge tracking of instantaneous LIF images. The results support our previous hypothesis [21] in which heat release rate oscillations driven by interflame edge oscillations are canceled by fuel staging. The result of this phase cancelation is neutralization of the instability feedback loop formed between large-scale flame oscillations, heat release rate fluctuations, and acoustic energy flux, thus stabilizing the flame. Axisymmetric fuel staging was found to produce a relatively higher degree of combustion stability as defined by local flame edge oscillation RMS, local flame edge oscillation phase offset, and dump plane pressure intermittency and RMS. This difference in nozzle staging efficacy is attributed to minor hardware variations between nozzles and replicates the results of our previous chemiluminescence imaging-based study [23].

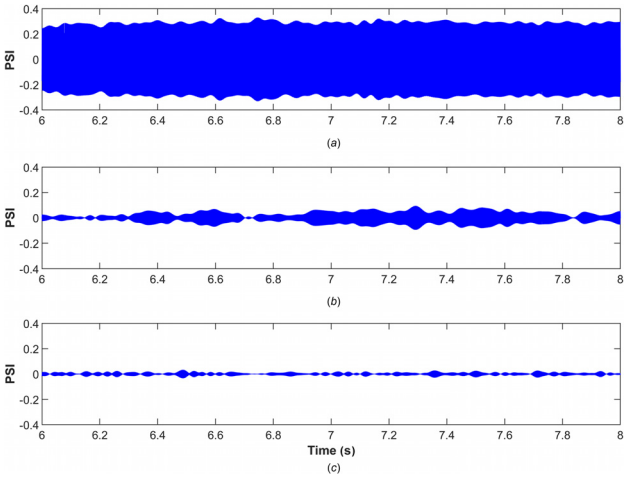


**Fig. 9 Dump plane pressure time series for (*a*) unstable unstaged, (*b*) right-nozzle staged, and (*c*) center-nozzle staged operating modes**

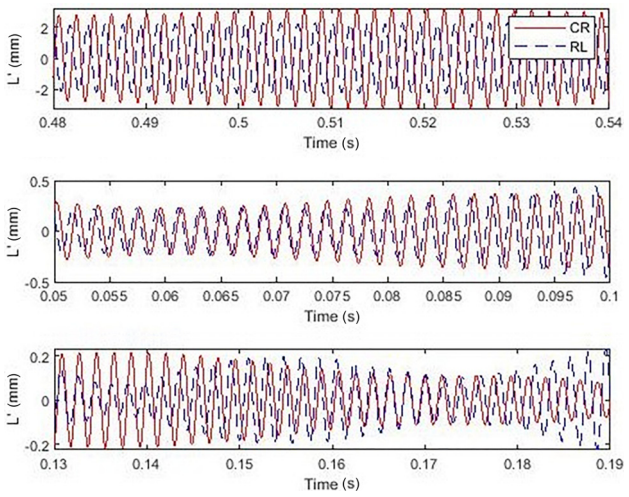


**Fig. 10 Center flame right branch (CR) and right flame left branch (RL) $L'$ time series for (*a*) unstaged unstable, (*b*) right-nozzle staged, and (*c*) center-nozzle staged operating modes**

## Acknowledgment

The authors would like to thank Olivia Sekulich for helping to check the accuracy of the edge-finding algorithm, and Dr. Keith McManus and Dr. Janith Samarasinghe of GE Global Research

for their input to this work throughout the duration of the project. The authors also wish to thank the U.S. Department of Energy for funding this work under award number DE-FE0025495 and contract monitor Mark Freeman.

## Nomenclature

P = pressure fluctuation
RMS = root-mean-square
$L'$ = instantaneous flame edge location oscillation
CR branch = right branch of center flame
RL branch = left branch of right flame
$\varphi$ = phase of flame edge oscillation
$\Delta\varphi$ = phase offset between CR and RL branches

## References

[1] McDonell, V., 2016, "Lean Combustion in Gas Turbines," *Lean Combustion*, Academic Press, London, UK, pp. 147–201.
[2] Zinn, B., and Lieuwen, T., 2005, "Combustion Instabilities: Basic Concepts," *Combustion Instabilities in Gas Turbine Engines: Operational Experience, Fundamental Mechanisms, and Modeling*, AIAA, Reston, VA, pp. 3–24.
[3] Rayleigh, J. W. S., 1878, "The Explanation of Certain Acoustical Phenomena," Nature, **18**, pp. 319–321.
[4] Richards, G., and Straub, D., 2005, "Passive Control of Combustion Instabilities in Stationary Gas Turbines," *Combustion Instabilities in Gas Turbine Engines: Operational Experience, Fundamental Mechanisms, and Modeling*, T. Lieuwen and V. Yang Eds., AIAA, Reston, VA, pp. 533–575.
[5] McManus, K., Poinsot, T., and Candel, S., 1993, "A Review of Active Control of Combustion Instabilities," Prog. Energy Combust. Sci., **19**(1), pp. 1–29.
[6] Herrmann, J., and Hoffmann, S., 2005, "Implementation of Active Control in a Full-Scale Gas-Turbine Combustor," *Combustion Instabilities in Gas Turbine Engines: Operational Experience, Fundamental Mechanisms, and Modeling*, T. Lieuwen and V. Yang Eds., AIAA, Reston, VA, pp. 611–633.
[7] Bulat, G., Skipper, D., McMillan, R., and Syed, K., 2007, "Active Control of Fuel Splits in Gas Turbine DLE Combustion Systems," ASME Paper No. GT2007-27266.
[8] Davis, L., and Black, S., 2000, "Dry Low $NO_x$ Combustion Systems for GE Heavy Duty Gas Turbines," GE Publication, Report No. GER-3568G.
[9] Li, L., Sun, X., Lioi, C., and Yang, V., 2017, "Effect of Azimuthally Nonuniform Heat Release on Longitudinal Combustion Instabilities," J. Propul. Power, **33**(1), pp. 193–203.
[10] Cohen, J., Hagen, G., Banaszuk, A., Becz, S., and Mehta, P., 2011, "Attenuation of Combustor Pressure Oscillations Using Symmetry Breaking," AIAA Paper No. 2011–0060.
[11] Noiray, N., Bothien, M., and Schuermans, B., 2011, "Investigation of Azimuthal Staging Concepts in Annular Gas Turbines," Combust. Theory Model., **15**(5), pp. 585–606.
[12] Noiray, N., and Schuermans, B., 2012, "On the Dynamic Nature of Azimuthal Thermoacoustic Modes in Annular Gas Turbine Combustion Chambers," Proc. R. Soc. A, **469**.
[13] Ghirardo, G., and Juniper, M., 2013, "Azimuthal Instabilities in Annular Combustors: Standing and Spinning Modes," Proc. R. Soc. A, **469**.
[14] Acharya, V., Bothien, M., and Lieuwen, T., 2018, "Non-Linear Dynamics of Thermoacoustic Eigen-Mode Interactions," Combust. Flame, **194**, pp. 309–321.
[15] Li, C., Yang, D., Li, S., and Zhu, M., 2018, "An Analytical Study of the Effect of Flame Response to Simultaneous Axial and Transverse Perturbations on Azimuthal Thermoacoustic Modes in Annular Combustors," Proc. Combust. Inst., **37**(4), pp. 5279–5287.
[16] Dawson, J., and Worth, N., 2014, "Flame Dynamics and Unsteady Heat Release Rate of Self-Excited Azimuthal Modes in an Annular Combustor," Combust. Flame, **161**(10), pp. 2565–2578.
[17] Kunze, K., Hirsch, C., and Sattelmayer, T., 2004, "Transfer Function Measurements on a Swirl Stabilized Premix Burner in an Annular Combustion Chamber," ASME Paper No. GT2004-53106.
[18] Aguilar, M., Malanoski, M., Adhitya, G., Emerson, B., Acharya, V., Noble, D., and Lieuwen, T., 2015, "Helical Flow Disturbances in a Multinozzle Combustor," ASME J. Eng. Gas Turbines Power, **137**(9), p. 091507.
[19] Worth, N., Dawson, J., Sidey, J., and Mastorakos, E., 2017, "Azimuthally Forced Flames in an Annular Combustor," Proc. Combust. Inst., **36**(3), pp. 3783–3790.
[20] Kwong, W., and Steinberg, A., 2019, "Blow-off and Reattachment Dynamics of a Linear Multinozzle Combustor," ASME J. Eng. Gas Turbines Power, **141**(1), p. 011015.
[21] Samarasinghe, J., Culler, W., Quay, B., Santavicca, D., and O'Connor, J., 2017, "The Effect of Fuel Staging on the Structure and Instability Characteristics of Swirl-Stabilized Flames in a Lean Premixed Multinozzle Can Combustor," ASME J. Eng. Gas Turbines Power, **139**(12), p. 121504.
[22] Culler, W., Chen, X., Peluso, S., Santavicca, D., and O'Connor, J., 2017, "The Effect of Transient Fuel Staging on Self-Excited Instabilities in a Multi-Nozzle Model Gas Turbine Combustor," ASME Paper No. GT2017-63479.
[23] Culler, W., Samarasinghe, J., Quay, B., Santavicca, D., O'Connor, J., and Noble, D., 2018, "Comparison of Center Nozzle Staging to Outer Nozzle Staging in a Multi-Flame Combustor," ASME Paper No. GT2018-75423.
[24] Lee, J., and Santavicca, D., 2003, "Experimental Diagnostics for the Study of Combustion Instabilities in Lean Premixed Combustors," J. Propul. Power, **19**(5), pp. 735–750.
[25] Orawannukul, P., 2014, "An Experimental Study of Forced Flame Response in Technically Premixed Flames in a Lean Premixed Gas Turbine Combustor," Ph.D. thesis, The Pennsylvania State University, State College, PA.
[26] Gonzalez, R., and Woods, R., 2007, *Digital Image Processing*, Prentice Hall, Upper Saddle River, NJ.
[27] Ducruix, S., Schuller, T., Durox, D., and Candel, S., 2003, "Combustion Dynamics and Instabilities: Elementary Coupling and Driving Mechanisms," J. Propul. Power, **19**(5), pp. 722–734.
[28] Shanbhogue, S., Shin, D.-H., Hemchandra, S., Plaks, D., and Lieuwen, T., 2009, "Flame-Sheet Dynamics of Bluff-Body Stabilized Flames During Longitudinal Acoustic Forcing," Proc. Combust. Inst., **32**(2), pp. 1787–1794.
[29] Samarasinghe, J., Peluso, S., Szedlmayer, M., De Rosa, A., Quay, B., and Santavicca, D., 2013, "Three-Dimensional Chemiluminescence Imaging of Unforced and Forced Swirl-Stabilized Flames in a Lean Premixed Multi-Nozzle Can Combustor," ASME J. Eng. Gas Turbines Power, **135**(10), p. 101503.
[30] Shin, D.-H., Plaks, D., and Lieuwen, T., 2011, "Dynamics of a Longitudinally Forced, Bluff Body Stabilized Flame," J. Propul. Power, **27**(1), pp. 105–116.
[31] Emerson, B., Mondragon, U., Acharya, V., Shin, D.-H., Brown, C., McDonell, V., and Lieuwen, T., 2013, "Velocity and Flame Wrinkling Characteristics of a Transversely Forced, Bluff-Body Stabilized Flame, Part I: Experiments and Data Analysis," Combust. Sci. Technol., **185**(7), pp. 1056–1076.
[32] Acharya, V., Emerson, B., Mondragon, U., Shin, D.-H., Brown, C., McDonell, V., and Lieuwen, T., 2013, "Velocity and Flame Wrinkling Characteristics of a Transversely Forced, Bluff-Body Stabilized Flame—Part II: Flame Response Modeling and Comparison With Measurements," Combust. Sci. Technol., **185**(7), pp. 1077–1097.
[33] Preetham, H., Santosh., and Lieuwen, T., 2008, "Dynamics of Laminar Premixed Flames Forced by Harmonic Velocity Disturbances," J. Propul. Power, **24**(9), pp. 1390–1402.
[34] McGill, R., Tukey, J., and Larsen, W., 1978, "Variations of Box Plots," Am. Stat., **32**(1), p. 12–16.